

Theory of magnetic short-range order for itinerant electron systems

U. TRAPPER⁽¹⁾, D. IHLE⁽¹⁾ and H. FEHSKE⁽²⁾

⁽¹⁾Institut für Theoretische Physik, Universität Leipzig, D-04109 Leipzig, Germany

⁽²⁾Physikalisches Institut, Universität Bayreuth, D-95440 Bayreuth, Germany

October 28, 1996

Abstract

On the basis of the one-band t - t' -Hubbard model a self-consistent renormalization theory of magnetic short-range order (SRO) in the paramagnetic phase is presented combining the four-field slave-boson functional-integral scheme with the cluster variational method. Contrary to previous SRO approaches the SRO is incorporated at the saddle-point and pair-approximation levels. A detailed numerical evaluation of the theory is performed at zero temperature, where both the hole- and electron-doped cases as well as band-structure effects are studied. The ground-state phase diagram shows the suppression of magnetic long-range order in favour of a paramagnetic phase with antiferromagnetic SRO in a wide doping region. In this phase the uniform static spin susceptibility increases upon doping up to the transition to the Pauli paraphase. Comparing the theory with experiments on high- T_c cuprates a good agreement is found.

PACS number(s): *75.10.-b, 71.28.+d, 71.45.-d*

1 Introduction

In the theory of strongly correlated itinerant electron systems two topics are of continued interest, namely (i) the localized–itinerant complementarity and (ii) the competition between magnetic long–range order (LRO) and short–range order (SRO). In particular, the concept of magnetic SRO and its interrelation to itinerant properties was investigated in the context of both narrow–band magnetism of transition metals and their compounds [1–6] and of the unconventional magnetic behaviour of high– T_c copper oxides [7–12]. In the cuprates, neutron scattering [13] and nuclear magnetic resonance experiments [14] reveal pronounced antiferromagnetic spin correlations within the CuO_2 planes which persist even in the superconducting phase. Moreover, measurements of the spin susceptibility $\chi(T, \delta)$ in the normal metallic state of $\text{La}_{2-\delta}\text{Sr}_\delta\text{CuO}_4$ (LSCO) [15, 16] show a maximum in the doping dependence as well as (for $\delta \lesssim 0.21$) in the temperature dependence and give further evidence for strong SRO effects at low temperatures, where the SRO decreases with increasing doping and temperature. Thus the experiments on cuprates bring out the importance of electron correlations as compared with the situation in traditional band magnetism, and therefore yield a new challenge for a microscopic theory of SRO in itinerant electron systems. Such a theory has to provide a self–consistent description of strong SRO (in the absence of LRO) down to zero temperature.

The previous theoretical approaches to the problem of SRO in transition metals and cuprates are mostly based on Hubbard–type models [1, 2, 4–6, 8–12, 17]. For example, to explain the normal–state susceptibility of LSCO in terms of SRO, the three–band Hubbard model was used [9]. In connection with the study of SRO some general problems have gained a renewed interest, such as the stability of various magnetic LRO phases against paraphases with and without SRO as well as the question of phase separation in strong correlation models [18, 12].

From the methodical point of view, the SRO theories for itinerant systems are preferentially formulated within functional–integral representations of the one–band Hubbard model using the static approximation. Thereby, various Hubbard–Stratonovich two–field methods, often combined with the single–site coherent potential approximation (CPA) [1, 2, 5, 6, 8] and,

in the context of high- T_c 's, the scalar four-field slave-boson approach [19, 9, 12] where employed. Those theories are designed to describe the formation and ordering of local magnetic moments in an *itinerant* system on a time scale large compared to the electron hopping time.

In the mode-mode coupling theory of spin fluctuations (SF) by Moriya *et al.* [1, 2] interpolating between the weakly magnetic (local SF in \vec{q} -space) and local moment (local SF in real space) limits, the SRO is reflected in the spatial correlation of thermal SF (with an amplitude increasing with temperature) and is appreciable even above the Curie temperature. Starting from the local moment limit and using the two-vector-field Hubbard-Stratonovich/CPA approach, the SRO is taken into account by an expansion in pairwise terms (within the bilinear approximation) around the *single-site* CPA saddle-point. The lack of self-consistency in this approach may be justified when the SRO is weak. Note that, at $T = 0$, the theory by Moriya *et al.* [1, 2] reduces to the Hartree-Fock approximation in both the weak- and strong-coupling limits, and the SRO is lost. The neglect of important correlations at zero temperature may be the reason for the absence of a maximum in the calculated spin susceptibility. Contrary, the phenomenological version of the interpolation theory given in Ref. [2] incorporates the SRO at the saddle point, and in the weakly magnetic limit the results of the classical approximation to the self-consistent renormalization theory of SF are recovered.

In the local-band theory of ferromagnetism [3, 4], where the fluctuations of the local magnetizations with a fixed amplitude are considered to be local in \vec{q} -space, the SRO is described by an expansion around the Stoner saddle point [4] and turns out to be strong near the Curie temperature. As in Ref. [1], the SRO-induced renormalization of the saddle point is disregarded.

The non-self consistency is also inherent in the SRO theories taking the SF to be local in real space and employing various cluster methods [5, 6, 8, 9]. For example, in the approaches of Refs. [6] and [9] resulting in an effective Ising free-energy functional, where the exchange energy is evaluated beyond the bilinear approximation used in Ref. [1] and is nearly independent on temperature, the SRO is treated by an expansion around the single-site CPA saddle-point and by the Bethe-Peierls approximation [20].

To sum up, all previous microscopic theories based on Hubbard–Stratonovich or slave–boson/CPA approaches do not take into account the SRO self–consistently. Just that, however, is needed when we are dealing with a *strong* SRO at *low* temperatures.

Besides the functional–integral techniques, there are only a few alternative methods concerned with the description of SRO [10, 11]. For example, to discuss the doping dependence of the zero–temperature susceptibility $\chi(0, \delta)$ in the one–band Hubbard model by a semi–phenomenological weak–coupling approach [11], it was argued that the susceptibility of an antiferromagnet with only SRO can be approximated by the perpendicular susceptibility of an antiferromagnet with LRO.

In previous work [12] we have briefly sketched an improved (non–CPA) treatment of SRO in the paraphase of the two–dimensional (2D) one–band Hubbard model, based on a four–field slave–boson (SB) functional–integral approach, by taking into consideration the feed–back effect of SRO on the saddle point. In the present paper our self–consistent renormalization theory of SRO, being valid also at $T = 0$, is presented and discussed in more detail. As compared with Ref. [12], the theory is improved methodically, and several extensions and new results are given. For example, we investigate the influence of the band structure and of both electron and hole dopings on the stability of magnetic SRO versus LRO and on the uniform static spin susceptibility in the paraphase.

The basic idea of our scenario for the occurrence of SRO in itinerant electron systems may be understood as follows. Measuring the ‘localization’ of the electron spins by the local (not thermally induced) magnetic moment, with increasing correlation strength, i.e. with increasing U/t and decreasing doping, the local moment increases. Concomitantly, local magnetizations develop and an effective exchange interaction will tend to align neighbouring local magnetizations antiferromagnetically, even in the absence of LRO. Of course, the occurrence of SRO depends on the doping level, and SRO effects become strongest at $T = 0$. That is, if the local–moment behaviour is sufficiently pronounced as compared with the itinerancy, a paraphase with antiferromagnetic SRO becomes energetically favourable. Let us emphasize that our SRO concept differs from that described, e.g., in Refs. [1, 2].

The paper is organized as follows. In Sec. 2, the action of the SB functional integral for the partition function of the one-band t - t' -Hubbard model on a square lattice (which may describe the essential features of low-energy charge and spin excitations in the cuprates [17]) is expressed in terms of fluctuating local magnetizations and internal magnetic fields and transformed to an effective generalized Ising model with exchange integrals of arbitrary range. The SRO is taken into account by the summation over the Ising spins within the cluster variational method (CVM) [21]. In Sec. 3, the resulting effective free-energy functional is treated in a non-local saddle-point approximation, where the SRO is incorporated, at an equal level of variational approximation, in a fully self-consistent way. Sec. 4 is devoted to the calculation of the uniform static spin susceptibility, where the analytical results on the influence of SRO are given within the Bethe-Peierls approximation. In Sec. 5, at $T = 0$, numerical results for the local magnetic moment and magnetization amplitude, the ground-state phase diagram, and the spin susceptibility as functions of both the hole and electron doping level and of the interaction strength are presented. Thereby, the influence of the band structure, as parameterized by the nearest- and next-nearest-neighbour transfer integrals, is studied. The summary of our work can be found in Sec. 6.

2 Effective free-energy functional for the Hubbard model

2.1 Slave-boson functional integral

In the scalar four-field SB representation [19] the Fock space at each site is enlarged by introducing the Bose fields e_i , $p_{i\sigma}$ and d_i describing projection operators onto empty, singly and doubly occupied states, respectively, and the Hubbard model is expressed as

$$\mathcal{H} = \sum_{ij\sigma} t_{ij} z_{i\sigma}^\dagger f_{i\sigma}^\dagger f_{j\sigma} z_{j\sigma} + U \sum_i d_i^\dagger d_i - h \sum_{i\sigma} \sigma f_{i\sigma}^\dagger f_{i\sigma} , \quad (2.1)$$

where t_{ij} are the transfer integrals between nearest ($-t$) and next-nearest ($-t'$) neighbours, h denotes the uniform external magnetic field, and

$$z_{i\sigma} = (1 - d_i^\dagger d_i - p_{i\sigma}^\dagger p_{i\sigma})^{-\frac{1}{2}} (e_i^\dagger p_{i\sigma} + p_{i-\sigma}^\dagger d_i) (1 - e_i^\dagger e_i - p_{i-\sigma}^\dagger p_{i-\sigma})^{-\frac{1}{2}} . \quad (2.2)$$

To exclude unphysical states in the extended Fock space, the local constraints

$$e_i^\dagger e_i + d_i^\dagger d_i + \sum_{\sigma} p_{i\sigma}^\dagger p_{i\sigma} = 1, \quad (2.3)$$

$$p_{i\sigma}^\dagger p_{i\sigma} + d_i^\dagger d_i = f_{i\sigma}^\dagger f_{i\sigma} \quad (2.4)$$

have to be fulfilled. Expressing the partition function \mathcal{Z} by a coherent–state functional integral over complex Bose ($\{b^{(*)}\}$; $b = e, p_{\sigma}, d$) and pseudofermionic Grassmann ($\{f, \bar{f}\}$) fields, the local constraints are enforced by the time–independent Lagrange multipliers $\lambda_i^{(1)}$ and $\lambda_{i\sigma}^{(2)}$. Integrating out the pseudofermions we have

$$\mathcal{Z} = \int [\mathcal{D}d^{(*)}][\mathcal{D}e^{(*)}][\mathcal{D}p_{\sigma}^{(*)}][d\lambda^{(1)}][d\lambda_{\sigma}^{(2)}] \exp \left\{ - \int_0^{\beta} d\tau \mathcal{L}(\tau) \right\}, \quad (2.5)$$

$$\begin{aligned} \mathcal{L}(\tau) = & \sum_i \left[e_i^* (\partial\tau + \lambda_i^{(1)}) e_i + \sum_{\sigma} p_{i\sigma}^* (\partial\tau + \lambda_i^{(1)} - \lambda_{i\sigma}^{(2)}) p_{i\sigma} \right. \\ & \left. + d_i^* \left(\partial\tau + \lambda_i^{(1)} - \sum_{\sigma} \lambda_{i\sigma}^{(2)} + U \right) d_i - \lambda_i^{(1)} \right] - \text{Tr} \ln \left[-G_{ij\sigma}^{-1}(\tau) \right] \end{aligned} \quad (2.6)$$

with

$$G_{ij\sigma}^{-1}(\tau) = (-\partial\tau + \mu - \lambda_{i\sigma}^{(2)} + \sigma h) \delta_{ij} - z_{i\sigma}^* z_{j\sigma} t_{ij}. \quad (2.7)$$

To remove the non–diagonal fluctuations in the transfer term of the inverse Green propagator (2.7), we employ the Shiba transformation [22]

$$G_{ij\sigma} \rightarrow \hat{G}_{ij\sigma} = \sum_{lm} \hat{z}_{il\sigma}^* G_{lm\sigma} \hat{z}_{mj\sigma}, \quad (2.8)$$

where $\hat{z}_{ij\sigma} = z_{i\sigma} \delta_{ij}$. Then, in the frequency representation of the Lagrangian (2.6), under the trace operation $G_{ij\sigma}^{-1}(\omega)$ can be replaced exactly by

$$\hat{G}_{ij\sigma}^{-1}(\omega + \mu) = \frac{\omega + \mu - \lambda_{i\sigma}^{(2)} + \sigma h}{q_{i\sigma}} \delta_{ij} - t_{ij} \quad (2.9)$$

with $q_{i\sigma} = |z_{i\sigma}|^2$. By a local $U(1)^{\otimes 3}$ gauge transformation the phases of the Bose fields e_i and $p_{i\sigma}$ are removed (radial gauge), and the Lagrange multipliers become time–dependent fields. Applying the static approximation for the bosons ($p_{i\sigma}, d_i, \lambda_{i\sigma}^{(2)}$, where the saddle–point approximation for $\lambda_i^{(1)}$ is used to eliminate the integrals over the e_i fields) and adopting the

transformed fields [23]

$$m_i = \sum_{\sigma} \sigma p_{i\sigma}^2, \quad \xi_i = -\frac{1}{2} \sum_{\sigma} \sigma \lambda_{i\sigma}^{(2)}, \quad (2.10)$$

$$n_i = \sum_{\sigma} p_{i\sigma}^2 + 2d_i^* d_i, \quad \nu_i = \frac{1}{2} \sum_{\sigma} \lambda_{i\sigma}^{(2)}, \quad (2.11)$$

the partition function is obtained as

$$\mathcal{Z} = \int [\mathcal{D}d][\mathcal{D}d^*][\mathcal{D}n][\mathcal{D}\nu][\mathcal{D}m][\mathcal{D}\xi] \exp \{-\beta\Psi(\{d, d^*, n, \nu, m, \xi\})\}, \quad (2.12)$$

$$\Psi = \sum_i (U d_i^* d_i - n_i \nu_i + m_i \xi_i) + \frac{1}{\pi} \int d\omega f(\omega - \mu) \text{Im Tr ln} \left[-\hat{G}_{ij\sigma}^{-1}(\omega) \right]. \quad (2.13)$$

In eqs. (2.10) and (2.11), m_i and n_i are the bosonic representations of the local magnetization and particle number, respectively, defined analogously to its fermionic counterparts $m_i^f = \sum_{\sigma} \sigma f_{i\sigma}^{\dagger} f_{i\sigma}$ and $n_i^f = \sum_{\sigma} f_{i\sigma}^{\dagger} f_{i\sigma}$. Since ξ_i couples to m_i as a magnetic field we denote ξ_i by ‘internal magnetic field’.

2.2 Transformation to a generalized Ising model

To incorporate the SRO beyond the *uniform* paramagnetic (PM) saddle point, we perform an expansion in terms of the local perturbation $V_{i\sigma} \delta_{ij} = -\hat{G}_{ij\sigma}^{-1} + \hat{G}_{ij\sigma}^{\circ-1}$, where

$$\hat{G}_{ij\sigma}^{\circ}(\omega) = \frac{q_{\sigma}^{\circ}}{N} \sum_{\vec{k}} \frac{e^{i\vec{k}(\vec{R}_i - \vec{R}_j)}}{\omega - E_{\vec{k}\sigma}^{\circ}} \quad (2.14)$$

is the PM saddle-point propagator with

$$E_{\vec{k}\sigma}^{\circ} = \lambda_{\sigma}^{\circ} - \sigma h + q_{\sigma}^{\circ} \varepsilon_{\vec{k}}, \quad (2.15)$$

$\lambda_{\sigma}^{\circ} = \nu^{\circ} - \sigma \xi^{\circ}$, and the 2D tight-binding band dispersion

$$\varepsilon_{\vec{k}} = -2t(\cos k_x + \cos k_y) - 4t' \cos k_x \cos k_y. \quad (2.16)$$

By the diagonal part of the Green propagator (2.14), the perturbation reads

$$V_{i\sigma}(\omega) = \left(1 - \frac{q_{\sigma}^{\circ}}{q_{i\sigma}}\right) \hat{G}_{ii\sigma}^{\circ-1}(\omega) + \frac{\lambda_{i\sigma}^{(2)} - \lambda_{\sigma}^{\circ}}{q_{i\sigma}}, \quad (2.17)$$

and we can split up the fermionic part of (2.13) as

$$\begin{aligned} \text{Tr} \ln \left[-\hat{G}_{ij\sigma}^{-1}(\omega) \right] &= \text{Tr} \ln \left[-\hat{G}_{ij\sigma}^{\circ-1}(\omega) \right] \\ &+ \text{Tr} \ln \left[(1 - \hat{G}_{ii\sigma}^{\circ}(\omega) V_{i\sigma}(\omega)) \delta_{ij} \right] \\ &+ \text{Tr} \ln \left[\delta_{ij} - \hat{G}_{(ij)\sigma}^{\circ}(\omega) T_{j\sigma}(\omega) \right]. \end{aligned} \quad (2.18)$$

Here, $T_{i\sigma} = V_{i\sigma} [1 - \hat{G}_{ii\sigma}^{\circ} V_{i\sigma}]^{-1}$ is the scattering matrix, and $\hat{G}_{(ij)\sigma}^{\circ}$ denotes the nondiagonal part of (2.14). The second term on the r.h.s. of (2.18) yields a single-site fluctuation contribution to the functional (2.13), whereas the third term describes the coupling between the fluctuations at all sites and is responsible for SRO effects.

Treating the fluctuations of the local magnetizations m_i and the internal magnetic fields ξ_i on an equal footing, we express those fields by their amplitude and direction according to

$$m_i = \bar{m}_i s_i, \quad \xi_i = \bar{\xi}_i s_i, \quad s_i = \pm 1. \quad (2.19)$$

Furthermore, we make the ansatz

$$b_i \rightarrow b_{s_i} \text{ with } b = \bar{m}, \bar{\xi}, n, \nu, d, d^*, \quad (2.20)$$

which becomes relevant for the calculation of the uniform static spin susceptibility (Sec. 4); for $h = 0$, we have $b_{s_i} = b$. In Appendix A the resulting partition function is transformed to that of an effective generalized Ising model along the lines indicated by Kakehashi [6]. In the pair approximation, where all terms of (2.18) involving more than two sites are neglected, we obtain

$$\mathcal{Z} = \sum_{\{s_i\}} \int [\mathcal{D}d_\alpha][\mathcal{D}d_\alpha^*][\mathcal{D}n_\alpha][\mathcal{D}\nu_\alpha][\mathcal{D}\bar{m}_\alpha][\mathcal{D}\bar{\xi}_\alpha] \exp\{-\beta\Psi(b_\alpha, \{s_i\})\} \quad (2.21)$$

with

$$\Psi(b_\alpha, \{s_i\}) = \bar{\Psi}(b_\alpha) + \Psi^{(\text{pair})}(b_\alpha, \{s_i\}), \quad (2.22)$$

$$\Psi^{(\text{pair})}(b_\alpha, \{s_i\}) = -\bar{h}(b_\alpha) \sum_i s_i - \sum_n \bar{J}_n(b_\alpha) \sum_{(ij)_n} s_i s_j. \quad (2.23)$$

Here, $\alpha = \pm 1$ and the index n denotes the n -th neighbour shell around a given lattice point i , where $(ij)_n$ sums over the z_n sites j in the n -th shell. The expressions for \bar{h} and the effective

Ising–exchange integrals \bar{J}_n are given in Appendix A. Let us emphasize that those quantities are complicated functions of all SB fields and have to be determined self–consistently at each interaction strength U and hole doping $\delta = 1 - n$.

Furthermore, remark that \bar{J}_n has to be contrasted from the effective Ising–exchange energy \tilde{J} occurring in previous Hubbard–Stratonovich/CPA approaches [6, 24], where \tilde{J} couples thermally induced local moments.

2.3 Cluster variational method

To perform the s_i –sum in the partition function (2.21) of the effective Ising model (2.23), we restrict ourselves to the square lattice and employ the CVM in the version given by Hijmans and de Boer [21]. In this method the calculation of the free energy in the (w) –cluster approximation starts from the choice of a basic cluster (w) and the series of subclusters (v) generated by overlapping two basic clusters in all possible ways, as illustrated in Fig. 1 [$(w) = (f)$, $(v) = (e), \dots, (a)$]. In the same way, the next generation of overlap figures can be obtained from each

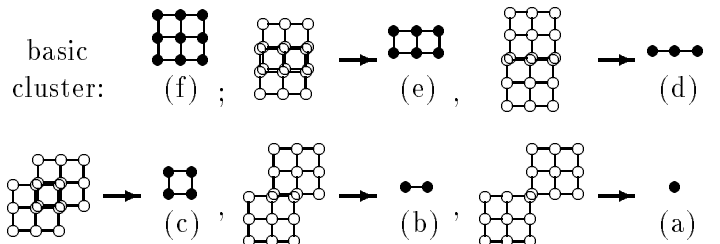


Fig. 1: Genesis of the series of subclusters (e) to (a) from the basic cluster (f) in the square lattice (see text).

of the subclusters (v) . Note that in each generation there occur ‘essential’ overlap figures [e.g., (e) in Fig. 1] which do not appear as overlap figures in the subsequent generations.

Following Ref. [21], the free energy of the N –site system in the (w) –cluster approximation is obtained as

$$\mathcal{F}_w(p_\kappa^{(w)}) = \sum_{v=a}^w y_w^{(v)} \mathcal{F}^{(v)}(p_{\kappa'}^{(v)}), \quad (2.24)$$

where

$$\mathcal{F}^{(v)}(p_{\kappa}^{(v)}) = N \sum_{\kappa \in (v)} \lambda_{\kappa}^{(v)} p_{\kappa}^{(v)} \left(\varepsilon_{\kappa}^{(v)} + \frac{1}{\beta} \ln p_{\kappa}^{(v)} \right) \quad (2.25)$$

is the free energy of an assembly of N independent clusters of type (v) . Here, κ labels the topologically inequivalent spin configurations of the cluster (v) with energy $\varepsilon_{\kappa}^{(v)}$ and the multiplicity $\lambda_{\kappa}^{(v)}$ (number of equivalent configurations of type κ), where $\varepsilon_{\kappa}^{(v)}$ and $\lambda_{\kappa}^{(v)}$ are calculated for an *isolated* cluster (v) . The distribution number $p_{\kappa}^{(v)}$ is the number of (v) -clusters with fixed configuration κ contained in a given configuration of the N -site lattice divided by the total number of (v) -clusters in the lattice, where the normalization condition

$$\sum_{\kappa \in (v)} \lambda_{\kappa}^{(v)} p_{\kappa}^{(v)} = 1 \quad (2.26)$$

has to be fulfilled. Of course, the distribution numbers $p_{\kappa}^{(v)}$ for the subcluster (v) are determined by the distribution numbers $p_{\kappa}^{(w)}$ for the chosen basic cluster (w) , i.e.

$$p_{\kappa}^{(v)} = p_{\kappa}^{(v)} [p_{\kappa'}^{(w)}], \quad \forall (v) \subset (w). \quad (2.27)$$

Since in the cluster construction of the total free energy in terms of the ‘microvariables’ $p_{\kappa}^{(v)} [p_{\kappa'}^{(w)}]$ described so far the different subclusters (v) are counted several times, in (2.24) the geometrical factors $y_w^{(v)}$ were introduced to compensate this overcounting and to give the correct number of (v) -clusters contributing to the free energy. In Appendix B the consistency relations (2.27) as well as the linear system of equations for $y_w^{(v)}$ are given in a more explicit form for the most simplest basic clusters (a) , (b) , and (c) .

Finally, in the spirit of the CVM, the free energy has to be minimized with respect to the ‘macrovariables’ $p_{\kappa}^{(w)}$. Since the constraint (2.26) also holds for the basic cluster (w) , we can reduce the variational degrees of freedom by one introducing, instead of the $p_{\kappa}^{(w)}$, a new set of independent variables x_{ι} . Accordingly, the CVM equations read

$$\frac{\partial \mathcal{F}_w(p_{\kappa}^{(w)}(x_{\iota}))}{\partial x_{\iota}} = 0. \quad (2.28)$$

It is worth emphasizing that alternatively all the CVM variables x_{ι} contained in \mathcal{F}_w can be expressed by the complete set of M -point ($M = 1, \dots, N^{(w)}$) correlation functions K belonging to the basic cluster (w) [25].

Applying this method to our spin model (2.23) we obtain the effective free–energy functional in the (w)–CVM approximation (c.f. Appendix B),

$$\begin{aligned} \Psi_w^{(\text{pair})}(b_\alpha, x_\iota) &= -N \left[K_{\bar{h}}(x_\iota) \bar{h}(b_\alpha) + \sum_n \frac{z_n}{2} K_{\bar{J}_n}(x_\iota) \bar{J}_n(b_\alpha) \right] \\ &+ N \sum_{v=a}^w y_w^{(v)} \sum_{\kappa \in (v)} \lambda_\kappa^{(v)} p_\kappa^{(v)}(x_\iota) \ln p_\kappa^{(v)}(x_\iota), \end{aligned} \quad (2.29)$$

where the internal energy part is given in terms of the expectation value

$$K_{\bar{h}} := \langle s_i \rangle = -\frac{1}{N} \frac{\partial \mathcal{F}_w}{\partial \bar{h}} \quad (2.30)$$

and of all pair–correlation functions in the basic cluster,

$$K_{\bar{J}_n} := \langle s_i s_j \rangle_n = -\frac{2}{z_n N} \frac{\partial \mathcal{F}_w}{\partial \bar{J}_n}. \quad (2.31)$$

In (2.29) the coupling to higher, e.g., 3–point or 4–point correlation functions results from the entropy term.

3 Saddle point with short–range order

Now we calculate the free energy per site

$$f(n, h, T) = \left[\frac{1}{\beta N} \mathcal{S} + \mu n \right] \Big|_{\text{SP}}, \quad (3.1)$$

where

$$\mathcal{S} = \beta \left[\bar{\Psi}(b_\alpha) + \Psi_w^{(\text{pair})}(b_\alpha, x_\iota) \right] \quad (3.2)$$

is the effective bosonic action, adopting the saddle–point and (w)–cluster variational approximations for all Bose fields b_α and variational parameters x_ι , respectively. Taking into account the dependences on b_α of $\bar{\Psi}$, \bar{h} and \bar{J}_n (cf. Appendix A), from $\partial \mathcal{S} / \partial b_\alpha = 0$ we get

$$\begin{aligned} \frac{1}{2} \sum_{\alpha'} \left\{ (1 + \alpha' K_{\bar{h}}) \left[\frac{\partial}{\partial b_\alpha} (U d_\alpha^* d_\alpha - n_\alpha \nu_\alpha + \bar{m}_\alpha \bar{\xi}_\alpha) + \sum_\sigma \frac{\partial \Phi_{\alpha\sigma}}{\partial b_\alpha} \right] \right. \\ \left. + \sum_{\substack{n \subseteq (w) \\ \sigma}} \frac{z_n}{4} \left[(1 + 2\alpha' K_{\bar{h}} + K_{\bar{J}_n}) \frac{\partial \Phi_{n, \alpha' \alpha' \sigma}}{\partial b_\alpha} + (1 - K_{\bar{J}_n}) \frac{\partial \Phi_{n, -\alpha' \alpha' \sigma}}{\partial b_\alpha} \right] \right\} = 0. \end{aligned} \quad (3.3)$$

This coupled system of self-consistency equations determining the saddle point with SRO can be cast to the form

$$\bar{m}_\alpha = \alpha \sum_\sigma \sigma n_{\alpha\sigma}^f, \quad \bar{\xi}_\alpha = - \sum_\sigma Q_{\alpha\sigma}^f \frac{\partial q_{\alpha\sigma}}{\partial \bar{m}_\alpha}, \quad (3.4)$$

$$n_\alpha = \sum_\sigma n_{\alpha\sigma}^f, \quad \nu_\alpha = \sum_\sigma Q_{\alpha\sigma}^f \frac{\partial q_{\alpha\sigma}}{\partial n_\alpha}, \quad (3.5)$$

$$U = - \sum_\sigma Q_{\alpha\sigma}^f \frac{\partial q_{\alpha\sigma}}{\partial d_\alpha^2}. \quad (3.6)$$

Here, $n_{\alpha\sigma}^f$ is the pseudofermionic expression for the particle density given by

$$n_{\alpha\sigma}^f = \frac{1}{1 + \alpha K_{\bar{h}}} \sum_{\alpha'} \left\{ (1 + \alpha' K_{\bar{h}}) \frac{\partial \Phi_{\alpha'\sigma}}{\partial \lambda_{\alpha\sigma}^{(2)}} + \sum_n \frac{z_n}{4} \left[(1 + 2\alpha' K_{\bar{h}} + K_{\bar{J}_n}) \frac{\partial \Phi_{n,\alpha'\alpha'\sigma}}{\partial \lambda_{\alpha\sigma}^{(2)}} + (1 - K_{\bar{J}_n}) \frac{\partial \Phi_{n,-\alpha'\alpha'\sigma}}{\partial \lambda_{\alpha\sigma}^{(2)}} \right] \right\}, \quad (3.7)$$

where $\lambda_{\alpha\sigma}^{(2)} = \nu_\alpha - \alpha\sigma\bar{\xi}_\alpha$. In eqs. (3.4) to (3.6), $Q_{\alpha\sigma}^f$ is given by (3.7) with $\partial\lambda_{\alpha\sigma}^{(2)}$ replaced by $\partial q_{\alpha\sigma}$. Finally, the chemical potential is determined from the number condition

$$n = 1 - \delta = \sum_{\alpha\sigma} p_\alpha^{(a)} n_{\alpha\sigma}^f \quad (3.8)$$

with

$$p_\alpha^{(a)} = \frac{1}{2}(1 + \alpha x_1). \quad (3.9)$$

At the saddle point, we have $n_{\alpha\sigma}^f = n_{\alpha\sigma} = (n_\alpha + \alpha\sigma\bar{m}_\alpha)/2$, where $n_{\alpha\sigma}$ is the bosonic expression. For vanishing local magnetization, $\bar{m}_\alpha = 0$, we have $V_{\alpha\sigma} = 0$ and (by (A.14) and (A.15)) $\bar{J}_n = 0$ so that there is no SRO, and the PM saddle point (with the external field h) is recovered from (3.4) to (3.6). Accordingly, in the $h = 0$ limit ($\bar{m}_\alpha = \bar{m}$; i.e., the integrals Φ in (3.7) only depend on $\eta = \alpha\sigma = \pm$) we obtain two possible paramagnetic phases: (i) the paraphase without SRO (PM) and (ii) the paraphase with magnetic SRO (SRO-PM), i.e.,

$$\begin{aligned} \text{PM} & : \langle s_i \rangle = 0, \quad \langle s_i s_j \rangle = 0; \quad \bar{m} = 0, \\ \text{SRO-PM} & : \langle s_i \rangle = 0, \quad \langle s_i s_j \rangle \neq 0; \quad \bar{m} > 0, \end{aligned} \quad (3.10)$$

where i and j are nearest-neighbour sites.

Let us stress that, at $T = 0$, the SRO–PM phase with antiferromagnetic correlations ($\langle s_i s_j \rangle < 0$; $\bar{J}_1 < 0$) must be distinguished from the phase with antiferromagnetic LRO (denoted by AFM) having a finite sublattice magnetization, $m_A = p_{A\uparrow}^2 - p_{A\downarrow}^2 = -m_B$, which is determined from the A–B saddle–point solution [26] and differs from the SRO amplitude \bar{m} ; in particular, we found $\bar{m} \neq 0$ in parameter regions, where $m_A = 0$ (see below, Fig. 2).

4 Spin susceptibility

The uniform static spin susceptibility $\chi = \lim_{h \rightarrow 0} \frac{dm}{dh}$, where $m = \sum_{\alpha} p_{\alpha}^{(a)} m_{\alpha}$ with $m_{\alpha} = \alpha \bar{m}_{\alpha}$ is the averaged magnetization, has to be calculated from

$$\chi = \lim_{h \rightarrow 0} \sum_{\alpha} \left(p_{\alpha}^{(a)} \frac{d m_{\alpha}}{d h} + m_{\alpha} \frac{d p_{\alpha}^{(a)}}{d h} \right), \quad (4.1)$$

using the solutions of the saddle–point and cluster variational equations for \bar{m}_{α} and $p_{\alpha}^{(a)}(x_1)$, respectively. The first term in (4.1) describes the change of the magnetization amplitude with the applied magnetic field and gives mainly the ‘itinerant’ contribution to χ . The second term describes directional fluctuations of the magnetizations and is called the ‘local’ contribution being finite only in the SRO–PM phase. However, note that the ‘itinerant’ and ‘local’ properties are interrelated and determine *both* contributions to the spin susceptibility.

Now we exploit the symmetry relations in the paraphase $\left. \frac{d \bar{m}_+}{d h} \right|_{h=0} \equiv \bar{m}_{+h} = -\bar{m}_{-h}$ and $\left. \frac{d \bar{\xi}_+}{d h} \right|_{h=0} \equiv \bar{\xi}_{+h} = -\bar{\xi}_{-h}$. Taking into consideration the full dependence on the external field h of the SB fields $[\bar{m}_+, \bar{\xi}_+, m^{\circ}, \xi^{\circ}]$ and variational parameters $[x_i]$, in the limit $h \rightarrow 0$ the uniform static spin susceptibility can be obtained from the solution of the following linear system of equations

$$\sum_i \mathcal{S}_{x_i y} x_{i h} + \mathcal{S}_{\bar{m}_{[+,-]y}} \bar{m}_{+h} + \mathcal{S}_{\bar{\xi}_{[+,-]y}} \bar{\xi}_{+h} + \mathcal{S}_{m^{\circ} y} m_h^{\circ} + \mathcal{S}_{\xi^{\circ} y} \xi_h^{\circ} = -\mathcal{S}_{h y}, \quad (4.2)$$

$$\mathcal{S}_{m^{\circ} y^{\circ}} m_h^{\circ} + \mathcal{S}_{\xi^{\circ} y^{\circ}} \xi_h^{\circ} = -\mathcal{S}_{h y^{\circ}}, \quad (4.3)$$

where $X_y = \left. \frac{\partial X}{\partial y} \right|_{h=0}$, $X_{x_{[+,-]}} = \left(\frac{\partial}{\partial x_+} - \frac{\partial}{\partial x_-} \right) X \Big|_{h=0}$, $X_{xy} = \left. \frac{\partial^2 X}{\partial x \partial y} \right|_{h=0}$ with $y = \bar{m}_+, \bar{\xi}_+, x_i$ and $y^{\circ} = m^{\circ}, \xi^{\circ}$.

In the paraphrase without SRO, from (4.3) we find

$$\xi_h^\circ = \frac{1 + \frac{1}{2}B\chi_1^\circ}{1 + A\chi_0^\circ + B\chi_1^\circ + \frac{1}{4}B^2(\chi_1^{\circ 2} - \chi_0^\circ\chi_2^\circ)} - 1, \quad (4.4)$$

and the susceptibility is

$$\chi_h^\circ := m_h^\circ = \frac{\chi_0^\circ}{1 + A\chi_0^\circ + B\chi_1^\circ + \frac{1}{4}B^2(\chi_1^{\circ 2} - \chi_0^\circ\chi_2^\circ)} \quad (4.5)$$

with

$$A = \sum_\sigma \frac{\partial^2 q_\sigma^\circ}{\partial m^{\circ 2}}, \quad B = \frac{1}{2} \sum_\sigma \sigma \frac{\partial q_\sigma^\circ}{\partial m^\circ}, \quad (4.6)$$

and the higher-order Lindhard functions

$$\chi_l^\circ = -\frac{1}{N} \sum_{\vec{k}\sigma} (2\varepsilon_{\vec{k}})^l \frac{\partial f(E_{\vec{k}\sigma}^\circ - \mu)}{\partial E_{\vec{k}\sigma}^\circ}. \quad (4.7)$$

Let us point out that our result for the spin susceptibility χ° agrees with the static and uniform limit of the dynamic spin susceptibility derived, within the spin-rotation-invariant SB scheme [27], from the Gaussian fluctuation matrix at the PM saddle point [28]. Contrary, the uniform static spin susceptibility given in Ref. [29] within the scalar four-field SB approach disagrees with the result of Li *et al.* [28] away from half-filling.

If we include magnetic SRO effects at the Bethe-Peierls level of approximation ($\iota = 1, 2$; cf. Appendix B), from the evaluation of (4.2) together with (4.4)–(4.7) we finally obtain the spin susceptibility as

$$\chi = \frac{\Theta_I \chi_I + \chi_{II}}{\Theta_I + \Theta_{II}}, \quad (4.8)$$

where

$$\chi_I = \Delta \left[\Xi \mathcal{S}_{\bar{m}_{[+, -] \bar{\xi}_+}} - \Lambda \mathcal{S}_{\bar{\xi}_{[+, -] \bar{\xi}_+}} \right], \quad (4.9)$$

$$\begin{aligned} \chi_{II} = & \beta \bar{m}_+ \Gamma + \beta \Delta \left\{ \left[\bar{m}_+ \left(\Xi \bar{h}_{\bar{m}_{[+, -]}} + \Lambda \bar{h}_{\bar{\xi}_{[+, -]}} \right) - \Gamma \mathcal{S}_{x_1 \bar{\xi}_+} \right] \mathcal{S}_{\bar{m}_{[+, -] \bar{\xi}_+}} \right. \\ & - \bar{h}_{\bar{\xi}_{[+, -]}} \left(\Lambda \mathcal{S}_{x_1 \bar{\xi}_+} - \Xi \mathcal{S}_{x_1 \bar{m}_+} \right) - \bar{m}_+ \Xi \bar{h}_{\bar{\xi}_{[+, -]}} \mathcal{S}_{\bar{m}_{[+, -] \bar{m}_+}} \\ & \left. + \left(\Gamma \mathcal{S}_{x_1 \bar{m}_+} - \bar{m}_+ \Lambda \bar{h}_{\bar{m}_{[+, -]}} \right) \mathcal{S}_{\bar{\xi}_{[+, -] \bar{\xi}_+}} \right\}, \quad (4.10) \end{aligned}$$

$$\Theta_I = 2 \exp\{-2\beta \bar{J}_1\} - 1, \quad (4.11)$$

$$\Theta_{\text{II}} = \beta\Delta \left[\left(\mathcal{S}_{x_1\bar{\xi}_+} \bar{h}_{\bar{m}_{[+,-]}} + \mathcal{S}_{x_1\bar{m}_+} \bar{h}_{\bar{\xi}_{[+,-]}} \right) \mathcal{S}_{\bar{m}_{[+,-]}\bar{\xi}_+} - \bar{h}_{\bar{\xi}_{[+,-]}} \mathcal{S}_{x_1\bar{\xi}_+} \mathcal{S}_{\bar{m}_{[+,-]}\bar{m}_+} - \bar{h}_{\bar{m}_{[+,-]}} \mathcal{S}_{x_1\bar{m}_+} \mathcal{S}_{\bar{\xi}_{[+,-]}\bar{\xi}_+} \right], \quad (4.12)$$

and

$$\Delta = \left[\mathcal{S}_{\bar{m}_{[+,-]}\bar{\xi}_+}^2 - \mathcal{S}_{\bar{\xi}_{[+,-]}\bar{\xi}_+} \mathcal{S}_{\bar{m}_{[+,-]}\bar{m}_+} \right]^{-1}, \quad (4.13)$$

$$\Xi = -S_{h\bar{\xi}_+} - \mathcal{S}_{m^o\bar{\xi}_+} m_h^o - \mathcal{S}_{\xi^o\bar{\xi}_+} \xi_h^o, \quad (4.14)$$

$$\Lambda = -S_{h\bar{m}_+} - \mathcal{S}_{m^o\bar{m}_+} m_h^o - \mathcal{S}_{\xi^o\bar{m}_+} \xi_h^o, \quad (4.15)$$

$$\Gamma = \bar{h}_h + \bar{h}_{m^o} m_h^o + \bar{h}_{\xi^o} \xi_h^o. \quad (4.16)$$

In this paper we are primarily interested in the zero-temperature susceptibility. Equations (4.8) to (4.16) then lead to

$$\lim_{T \rightarrow 0} \chi = \begin{cases} \chi_{\text{I}} & \text{for } \bar{J} < 0 \quad (\text{antiferromagnetic SRO}) \\ \chi^o & \text{for } \bar{J} \equiv 0 \quad (\text{PM}) \\ \frac{\chi_{\text{II}}}{\Theta_{\text{II}}} & \text{for } \bar{J} > 0 \quad (\text{ferromagnetic SRO}). \end{cases} \quad (4.17)$$

It is noteworthy that, in contrast to the theory by Baumgärtel *et al.* [9], we get a finite spin susceptibility at $T = 0$.

5 Numerical results and discussion

We have numerically solved the self-consistency equations (3.4) to (3.9) at $T = 0$, where the SRO is included within the Bethe-Peierls approximation, and the 2D tight-binding unperturbed density of states corresponding to (2.16) is used. To determine the magnetic ground-state properties (SRO versus LRO, susceptibility $\chi(0, \delta)$), all the SB fields b_α and CVM variables (x_1, x_2) are evaluated as functions of U/t and doping. Note that in the complicated numerics particular attention has to be paid to the analytical behaviour of the complex logarithm appearing in the integrals (A.5), (A.15) and in their derivatives.

The band structure is incorporated via the non-interacting dispersion (2.16), where we have chosen (besides $t' = 0$) the ratio $t'/t = -0.16$ according to ab-initio parameters for hole-doped ($\delta > 0$) LSCO [17] and ARPES data on electron-doped ($\delta < 0$) $\text{Nd}_{2-\delta}\text{Ce}_\delta\text{CuO}_4$ [30]. For both compounds, realistic values of U/t lie between $6 \lesssim U/t \lesssim 10$ [17].

5.1 Long-range order versus short-range order

Concerning the LRO ground states of the 2D t - t' -Hubbard model, within our *scalar* four-field SB approach resulting in an effective *Ising* free-energy functional, only antiferromagnetic (AFM) and ferromagnetic (FM) LRO may be described by the A-B and uniform saddle-point solutions, respectively [31, 26]. Up to $U/t = 10$ and for either doping level we do not obtain a FM phase. This should be qualitatively contrasted with the results obtained by Hartree-Fock approaches [32, 33], where FM states are found for doping regions with $U/t \gtrsim 5$. This discrepancy may be explained by the appearance of antiferromagnetic SRO which counteracts ferromagnetism (as in the SRO theories of finite-temperature magnetism, cf. Sec. 1) and which we have found to be stabilized for $U/t > 5 - 6$ (for details see below). The suppression of FM Hartree-Fock ground states by antiferromagnetic SRO is in accord with Quantum Monte Carlo (QMC) results [32].

To discuss the competition between antiferromagnetic LRO and antiferromagnetic SRO and to give more insight into our SRO concept, already described qualitatively in Sec. 1, let us first quantify the behaviour of various magnetic parameters as functions of hole and electron doping. In Fig. 2 the sublattice magnetization m_A in the AFM phase, the local-magnetization amplitude \bar{m} being finite only in the SRO-PM phase, where the SRO is found to be antiferromagnetic ($\bar{J}_1 < 0$), and the local magnetic moment $m_{loc} = \frac{3}{4}(n - 2d^2)$ are depicted. In the case $\delta < 0$ we have taken $U/t = 9$ (instead of $U/t = 8$ for $\delta > 0$), in order to get an SRO-PM phase at $t'/t = -0.16$. As can be seen, at large enough interaction strengths we obtain an AFM \rightleftharpoons SRO-PM phase transition of first order at a small critical doping δ_{c_1} (the thin dashed lines in Fig. 2 indicate m_A in the region, where the AFM solution becomes metastable) and a SRO-PM \rightleftharpoons PM transition of second order at δ_{c_2} .

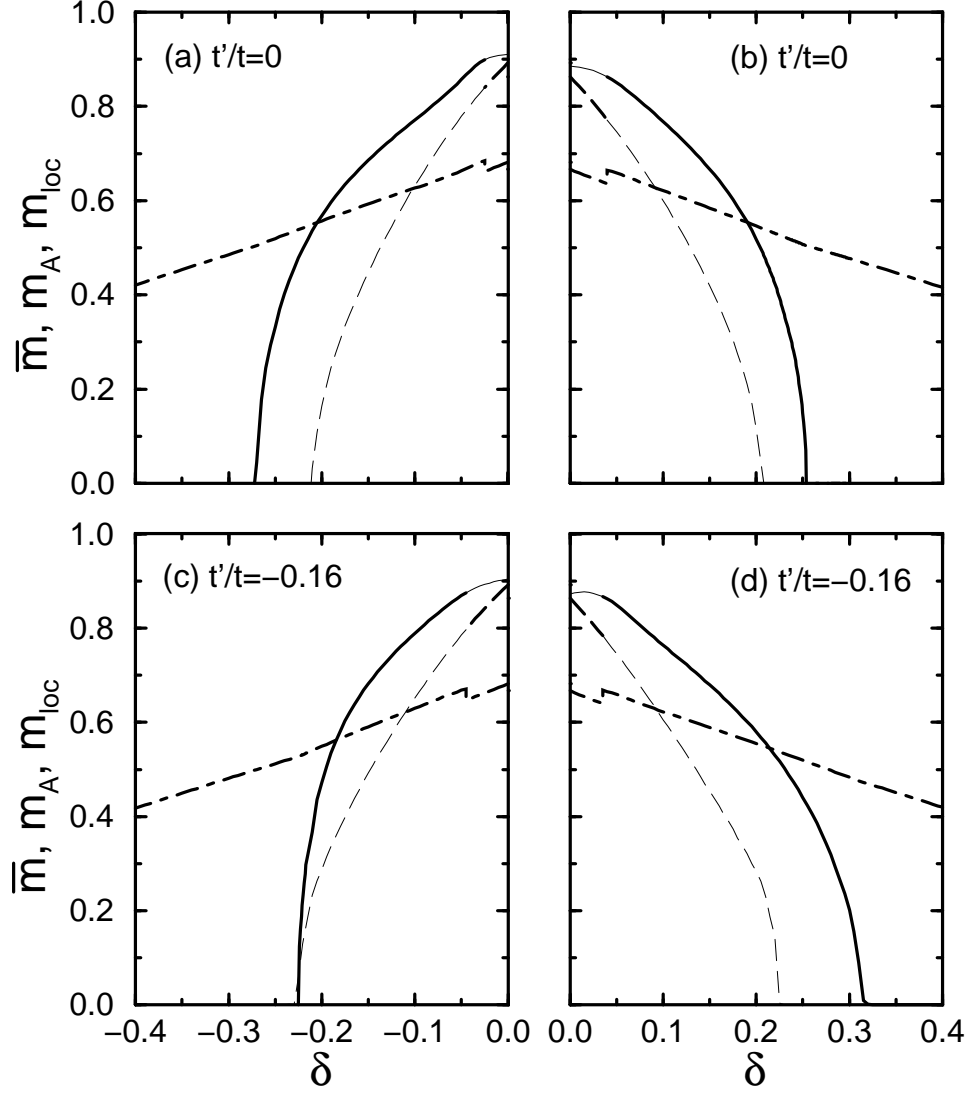


Fig. 2: Local-magnetization amplitude \bar{m} (solid curve) compared with the sublattice magnetization m_A (dashed line) and the local magnetic moment m_{loc} (chain-dashed line) as functions of electron doping ($U/t = 9$; **a,c**) and hole doping ($U/t = 8$; **b, d**). Note the electron-hole symmetry for $t' = 0$ and the asymmetry for $t' \neq 0$. The thin lines indicate the metastable solutions.

The local magnetic moment measures the ‘localization’ of the electron spins and, contrary to \bar{m} , is finite in the PM phase as well. With decreasing $|\delta|$ the correlation strength increases resulting in the increase of m_{loc} (as known from the theory of itinerant magnetism). If the

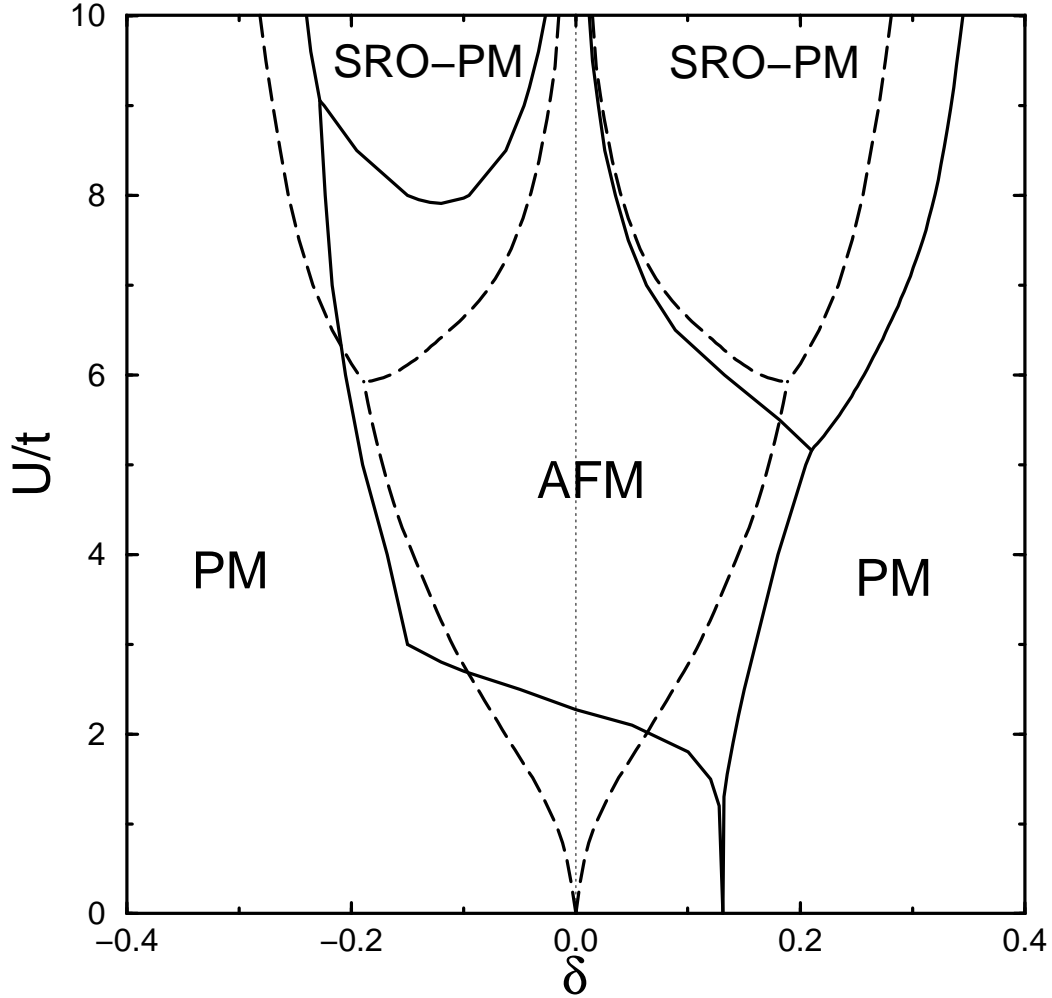


Fig. 3: Ground-state phase-diagram of the t - t' -Hubbard model, where AFM, PM, and SRO-PM denote the antiferromagnetic LRO phase, the paraphase without SRO, and the paraphase with SRO, respectively. The solid (dashed) lines mark the phase boundaries at $t'/t = -0.16$ ($t'/t = 0$).

'localization' prevails over the itinerancy, the formation of antiferromagnetic SRO is energetically favoured ($|\delta| < |\delta_{c_2}|$). Once the SRO has been established, m_{loc} is slightly enhanced with respect to its value in the PM state (cf. Fig. 2).

In the ground-state phase diagram of the 2D t - t' -Hubbard model shown in Fig. 3 one observes the suppression of LRO by SRO (at large enough U/t values) in a wide doping region. The energy comparison between the SRO-PM phase and various incommensurate spiral LRO

phases (obtained by the spin-rotation-invariant SB saddle-point solution [34]) was performed in our previous work [12] for the particular value $U/t = 8$, where also the problem of phase separation was discussed, and yields qualitatively the same SRO effects. For $U/t = 8$ (being realistic for LSCO) and $\delta > 0$ we get $\delta_{c_1} \simeq 0.04$ which agrees with the observed critical hole doping for the destruction of antiferromagnetism in LSCO. From this result we conclude that the rapid disappearance of antiferromagnetism in the quasi-2D hole-doped cuprates is related to the persistence of a strong 2D antiferromagnetic SRO in the paraphase.

For $t'/t = -0.16$ and $6 \lesssim U/t \lesssim 8$ the pronounced electron-hole asymmetry manifests itself in the stability of the AFM phase in a much wider electron doping region as compared with the hole-doped case. The t' -induced shrinking of the stability region of the SRO-PM phase in the $\delta < 0$ case originates from band-structure effects and, in particular, from the shift of the logarithmic Van-Hove singularity in the noninteracting density of states. Our findings are in accord with the asymmetry of the experimental phase diagram showing the disappearance of antiferromagnetism in $\text{Nd}_{2-\delta}\text{Ce}_\delta\text{CuO}_4$ at $\delta_{c_1} \simeq -0.15$.

In the hole-doped systems, the hopping along the square lattice diagonals favours antiferromagnetic correlations (Fig. 3) so that the SRO persists up to $\delta_{c_2} \simeq 30\%$ ($U/t \simeq 8$). Since just at this doping the superconductivity in LSCO disappears, we suggest that the antiferromagnetic SRO may be closely connected with the superconducting pairing mechanism in the hole-doped cuprates.

Let us now discuss the weak-interaction part of the phase diagram of the t - t' -Hubbard model, where only the PM \rightleftharpoons AFM phase transition may take place. At half-filling and $t' \neq 0$, this transition occurs at a non-zero critical value U_c rather than at $U = 0$ as for $t' = 0$; at $t'/t = -0.16$ (-0.2) we get $U_c/t = 2.3$ (2.5). This result agrees with the QMC value ($U_c/t = 2.5 \pm 0.25$) obtained at $t'/t = -0.2$ [32, 35] and may be explained by the shift of the position of the Van-Hove singularity for $t' \neq 0$ (for comparison, the Hartree-Fock calculation yields $U_c/t = 2.1$ [32]). A more detailed investigation of the half-filled t - t' -Hubbard model will be published elsewhere [36].

At the hole doping $\delta = 0.13$ and $t'/t = -0.16$ (see the phase diagram, Fig. 3), the AFM

state is stable against the FM state down to $U = 0$ which qualitatively agrees with the Hartree–Fock result of Ref. [32], but contradicts the result obtained by Brenig [33]. Thus, the correct weak–interaction limit of our saddle–point solution is confirmed.

Let us stress again that at large interaction strengths ($U/t > 5$) the appearance of SRO, in addition to the inclusion of an appreciable part of the correlations at the SB–PM saddle point, changes the phase diagram qualitatively as compared with any Hartree–Fock solution, in particular, the FM and AFM LRO states are suppressed in a wide doping region.

5.2 Spin susceptibility and short–range order

Based on the solution of the self–consistency equations discussed above, in the PM and SRO–PM phases we have evaluated the doping dependence of the zero–temperature susceptibility $\chi(0, \delta)$ according to the theory presented in Sec. 4.

Figure 4 shows our results for the electron– and hole–doped cases at large interaction strengths, where the SRO–PM phase is stabilized (cf. Fig. 3). In the PM phase, the Pauli susceptibility of the SB–renormalized tight–binding band reveals a pronounced increase with decreasing (electron or hole) doping which notably depends on t'/t . This behaviour may be ascribed to Fermi–surface topology effects. Beyond the PM=SRO–PM transition at δ_{c_2} (cf. Fig. 3), the Pauli susceptibility is suppressed due to the antiferromagnetic–SRO–induced spin stiffness against the orientation of the local magnetizations along the direction of the homogeneous external magnetic field. Correspondingly, at δ_{c_2} a cusp in $\chi(0, \delta)$ appears. According to the phase diagram, with increasing U/t the PM=SRO–PM transition shifts to higher doping levels so that the peak position in $\chi(0, \delta)$ reveals the same U/t dependence. Analogously, from Fig. 3 the t' dependence of the peak position emerges. With decreasing doping the degree of SRO or, equivalently, the magnitude of the antiferromagnetic exchange energy, $|\bar{J}_1|$, increases [12] so that the susceptibility decreases.

In the low–doping regime ($|\delta| \gtrsim |\delta_{c_1}|$), where the SRO is most pronounced and the ‘local’ contribution to the susceptibility (4.1) predominates the ‘itinerant’ contribution, the absolute value of $\chi(0, \delta)$ may appreciably depend on the chosen approach in describing the local pro-

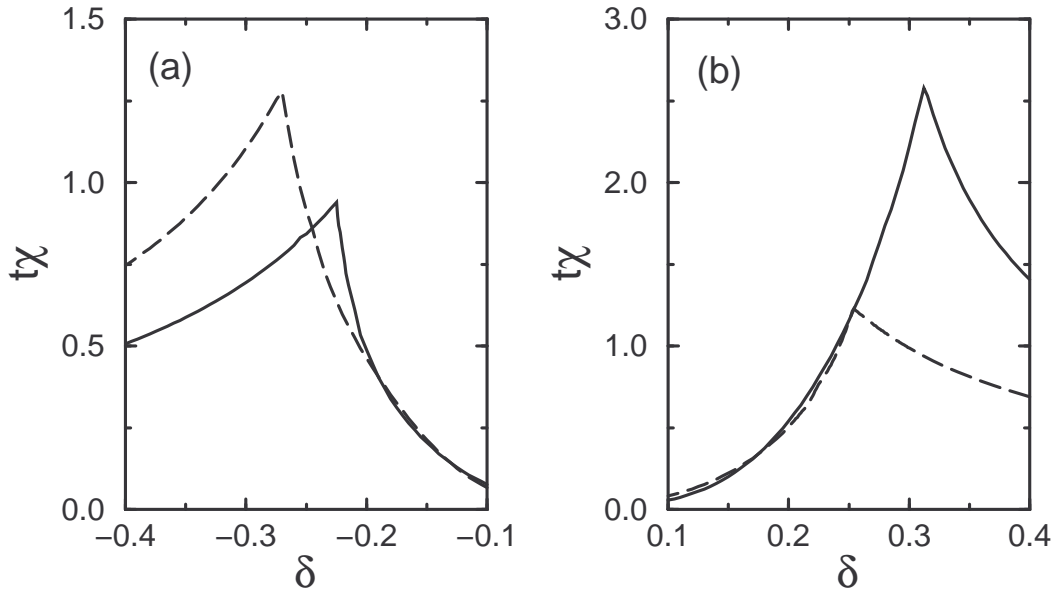


Fig. 4: Uniform static spin susceptibility at $T = 0$ as a function of electron doping ($U/t = 9$; **a**) and hole doping ($U/t = 8$; **b**) for $t'/t = -0.16$ (solid) and $t'/t = 0$ (dashed).

properties for the following reason. In our scalar SB approach the local properties are treated on the basis of an effective Ising functional, describing longitudinal magnetization fluctuations only, which yields an Ising-type ‘local’ contribution to χ . However, an improved SRO theory based on the spin-rotation-invariant SB scheme [27] results in an effective Heisenberg functional including the transverse fluctuations too [37]. As known from the pure Heisenberg model [38], the finite value of the zero-temperature susceptibility (being proportional to the inverse exchange coupling) is due to the transverse spin fluctuations. Therefore, we suggest that a spin-rotation-invariant theory of SRO describing the interrelation between a Heisenberg-type ‘local’ and ‘itinerant’ contribution to the susceptibility may enhance the magnitude of χ in the low-doping region as compared with our results shown in Fig. 4.

In Fig. 5 we have depicted the zero-temperature susceptibility calculated for the t - t' -Hubbard model taking realistic parameter sets for LSCO [17] without using any fit procedure in comparison with experiments on the spin contribution to the magnetic susceptibility of LSCO at 50 K [15, 16]. This contribution is obtained from the experimental data on the

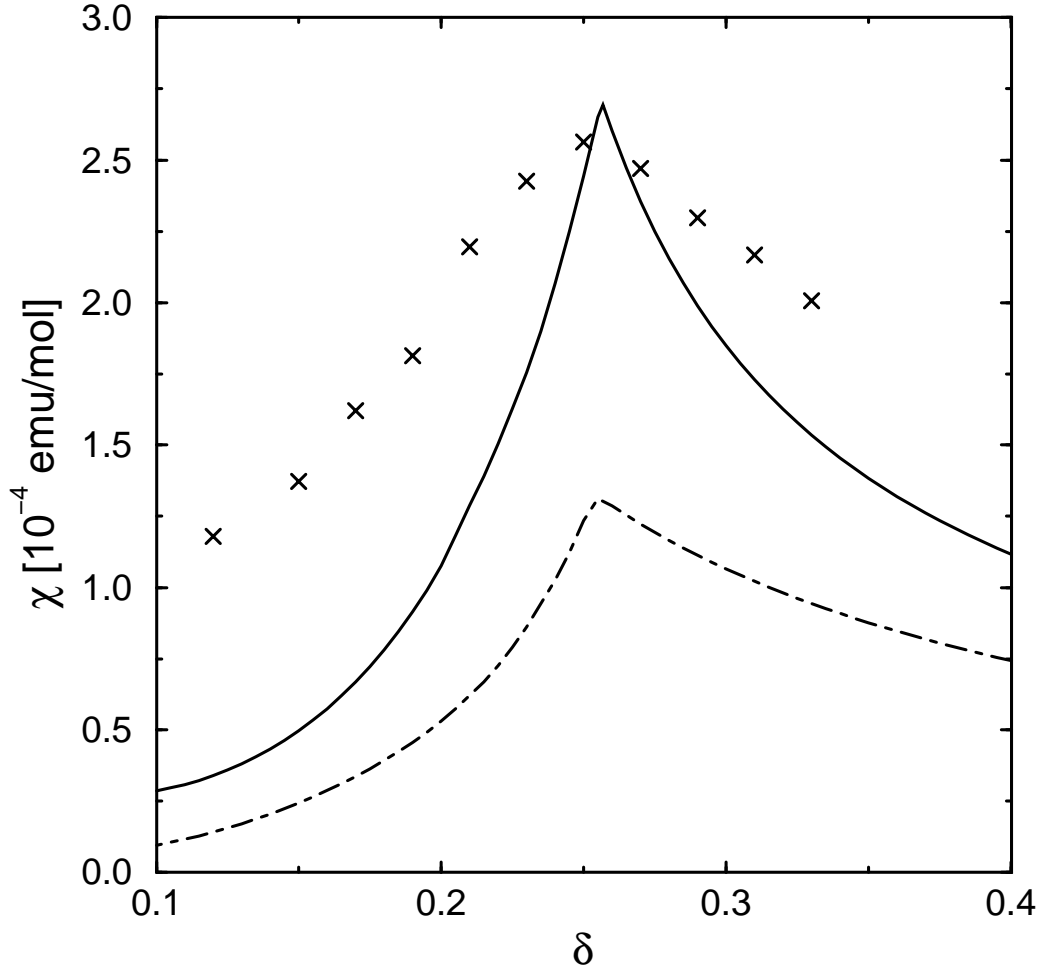


Fig. 5: Uniform static spin susceptibility at $T = 0$ as a function of hole doping. The theoretical results obtained for the 2D Hubbard model at $U/t = 6$, $t'/t = -0.16$ (solid) and $U/t = 8$, $t'/t = 0$ (chain-dashed), where the realistic value $t = 0.3$ eV is taken, are compared with the spin contribution (\times) to the (corrected) experimental susceptibility of $\text{La}_{2-\delta}\text{Sr}_\delta\text{CuO}_4$ at $T = 50$ K (Refs. [15] and [16]).

total susceptibility [15] by subtracting the diamagnetic core (-9.9×10^{-5} emu/mol) and Van Vleck (2.4×10^{-5} emu/mol) contributions which, according to Ref. [16], can be taken as independent of doping and temperature over the limited parameter region studied here. As Fig. 5 shows, our SRO theory reproduces very well the position and, for suitable realistic parameters, even the height of the observed pronounced susceptibility maximum at a hole

doping of about 25%. Moreover, the qualitative doping dependence of χ is in reasonable agreement with experiments. However, in the low-doping region, the theoretical susceptibility is too low as compared with experiments. This deficiency may be ascribed to the neglect of transverse magnetization fluctuations, as discussed above.

Finally, we notice that the increase of the spin susceptibility upon doping, explained by our theory as an SRO effect in the one-band t - t' -Hubbard model at $U/t > 5-6$, is in qualitative accord with recent QMC data [39] and with results on the one-band Hubbard model ($t' = 0$) based on a semi-phenomenological approach [11] and on the composite-operator method [40]. In those works a maximum in the spin susceptibility was found even at a smaller coupling ($U/t = 4$).

6 Summary

In this paper we have developed a theory of magnetic short-range order (SRO) in itinerant electron systems on the basis of the one-band t - t' -Hubbard model. The slave-boson functional-integral method was improved, as compared with previous approaches [1, 2, 4-6, 8, 9], by taking into consideration the self-consistent renormalization of the paramagnetic saddle point by SRO. The basic ingredients of our (non-CPA) theory are the following.

- (i) The four field slave-boson functional-integral representation is used to include an appreciable part of the correlations already at the uniform paramagnetic (PM) saddle point.
- (ii) The SRO of local magnetizations is incorporated beyond the PM saddle point within an effective generalized Ising model treated by means of the cluster variational method (CVM). The CVM is illustrated by cluster approximations with successively increasing sizes of the basic cluster.
- (iii) The SRO saddle point is determined from the free-energy functional by minimization with respect to all Bose fields and CVM variables.
- (iv) The inclusion of a homogeneous external magnetic field at the SRO saddle point allows the self-consistent calculation of SRO effects on the uniform static spin susceptibility.

The theory is numerically evaluated at $T = 0$, where the SRO is taken into account at the Bethe–Peierls level of approximation. The dependence of SRO effects on the interaction strength, the hole and electron doping and on the band structure (modeled by t'/t) is investigated. The main results are summarized as follows.

- (i) At $5 < U/t < 10$ ($t'/t = -0.16$) and for any doping level, the ferromagnetic long-range order (LRO) obtained in previous Hartree–Fock calculations [32] is suppressed due to the appearance of antiferromagnetic SRO.
- (ii) The antiferromagnetic and incommensurate spiral LRO phases obtained by mean-field-type approaches make way to a paraphase with antiferromagnetic SRO in a wide doping region. In the ground-state phase diagram, a pronounced t' -induced electron–hole asymmetry is observed.
- (iii) The uniform static spin susceptibility increases upon doping in the SRO–PM phase and shows a cusp at the transition to the Pauli paraphase.

From the good quantitative agreement of our theory with experiments on cuprates we conclude that the concept of a strong SRO in electron correlation models for high- T_c compounds may play an important role in the explanation of many unconventional magnetic properties and of the superconducting pairing mechanism in high T_c 's.

Acknowledgements

This work was performed under the auspices of Deutsche Forschungsgemeinschaft under project SF–HTSL–SRO. U.T. acknowledges the hospitality at the University of Bayreuth.

Appendix A: Effective Ising model

According to the reasonings in Sec. 2.2, by the use of (2.18) to (2.20) the functional (2.13) is expanded as

$$\Psi(\{b_{s_i}, s_i\}) = \Psi^{(0)} + \Psi^{(1)}(\{b_{s_i}, s_i\}) + \Psi^{(N)}(\{b_{s_i}, s_i\}) \quad (\text{A.1})$$

with

$$\Psi^{(0)} = \frac{1}{\beta} \sum_{\vec{k}\sigma} \ln \left[1 - f(E_{\vec{k}\sigma}^o - \mu) \right] \quad (\text{A.2})$$

and the single-site and N -site fluctuation contributions,

$$\Psi^{(1)}(\{b_{s_i}, s_i\}) = \sum_i \left(U d_{s_i}^* d_{s_i} - n_{s_i} \nu_{s_i} + \bar{m}_{s_i} \bar{\xi}_{s_i} + \sum_{\sigma} \Phi_{i\sigma}(b_{s_i}, s_i) \right) \quad (\text{A.3})$$

and

$$\Psi^{(N)}(\{b_{s_i}, s_i\}) = \int d\omega f(\omega - \mu) \frac{1}{\pi} \text{Im} \text{Tr} \ln \left[\delta_{ij} - \hat{G}_{(ij)\sigma}^o T_{j\sigma}(b_{s_j}, s_j) \right], \quad (\text{A.4})$$

respectively, where

$$\Phi_{i\sigma}(b_{s_i}, s_i) = \int d\omega f(\omega - \mu) \frac{1}{\pi} \text{Im} \ln \left[1 - \hat{G}_{ii\sigma}^o V_{i\sigma}(b_{s_i}, s_i) \right]. \quad (\text{A.5})$$

Using the identity

$$\Psi(\{b_{s_i}, s_i\}) = \sum_{\{\alpha_i = \pm\}} \left(\prod_i \frac{1 + s_i \alpha_i}{2} \right) \Psi(\{b_{\alpha_i}, \alpha_i\}) \quad (\text{A.6})$$

we get

$$\Psi(\{b_{s_i}, s_i\}) = \bar{\Psi} - \sum_i \bar{h}_i s_i - \sum_{(ij)} \bar{J}_{ij} s_i s_j - \sum_{(ijk)} \dots \quad (\text{A.7})$$

with

$$\bar{\Psi}(b_{\alpha_i}) = \left(\frac{1}{2}\right)^N \sum_{\{\alpha_i\}} \Psi(\{b_{\alpha_i}, \alpha_i\}), \quad (\text{A.8})$$

$$\bar{h}_i(b_{\alpha_i}) = -\left(\frac{1}{2}\right)^N \sum_{\{\alpha_i\}} \alpha_i \Psi(\{b_{\alpha_i}, \alpha_i\}), \quad (\text{A.9})$$

$$\bar{J}_{ij}(b_{\alpha_i}, b_{\alpha_j}) = -\left(\frac{1}{2}\right)^N \sum_{\{\alpha_i\}} \alpha_i \alpha_j \Psi(\{b_{\alpha_i}, \alpha_i\}). \quad (\text{A.10})$$

Treating (A.4) in the pair approximation we have

$$\text{Tr} \ln \left[\delta_{ij} - \hat{G}_{(ij)\sigma}^o T_{j\sigma}(b_{\alpha_j}, \alpha_j) \right] = \sum_{(ij)\sigma} \ln \left[1 - \hat{G}_{(ij)\sigma}^o T_{j\sigma}(b_{\alpha_j}, \alpha_j) \hat{G}_{(ji)\sigma}^o T_{i\sigma}(b_{\alpha_i}, \alpha_i) \right], \quad (\text{A.11})$$

and the higher order terms in (A.7) vanish. Then, the functional (A.7) takes the form of the generalized Ising model (2.23), where the effective parameters are given by

$$\bar{\Psi}(b_\alpha) = \Psi^{(0)} + \frac{N}{2} \sum_{\alpha} \left\{ U d_{\alpha}^* d_{\alpha} - n_{\alpha} \nu_{\alpha} + \bar{m}_{\alpha} \bar{\xi}_{\alpha} + \sum_{\sigma} \left[\Phi_{\alpha\sigma} + \frac{1}{4} \sum_n z_n (\Phi_{n,\alpha\alpha\sigma} + \Phi_{n,-\alpha\alpha\sigma}) \right] \right\}, \quad (\text{A.12})$$

$$\bar{h}(b_\alpha) = -\frac{1}{2} \sum_{\alpha} \alpha \left[U d_{\alpha}^* d_{\alpha} - n_{\alpha} \nu_{\alpha} + \bar{m}_{\alpha} \bar{\xi}_{\alpha} + \sum_{\sigma} \left(\Phi_{\alpha\sigma} + \frac{1}{2} \sum_n z_n \Phi_{n,\alpha\alpha\sigma} \right) \right], \quad (\text{A.13})$$

$$\bar{J}_n(b_\alpha) = -\frac{1}{4} \sum_{\alpha\sigma} (\Phi_{n,\alpha\alpha\sigma} - \Phi_{n,-\alpha\alpha\sigma}). \quad (\text{A.14})$$

Here, $\Phi_{\alpha\sigma} = \Phi_{i\sigma}(\alpha_i)|_{\alpha_i=\alpha}$, and $\Phi_{n,\alpha\alpha'\sigma} = \Phi_{(ij)_n\sigma}(\alpha_i, \alpha_j)|_{\substack{\alpha_i=\alpha \\ \alpha_j=\alpha'}}$ with

$$\Phi_{(ij)_n\sigma} = \int d\omega f(\omega - \mu) \frac{1}{\pi} \text{Im} \ln \left[1 - \hat{G}_{(ij)_n\sigma}^{\circ} T_{j\sigma}(b_{\alpha_j}, \alpha_j) \hat{G}_{(ji)_n\sigma}^{\circ} T_{i\sigma}(b_{\alpha_i}, \alpha_i) \right] \quad (\text{A.15})$$

is the two-site fluctuation contribution which takes into account SRO effects.

Appendix B: Cluster variational method and examples

To illustrate the algorithm of the CVM sketched in Sec. 2.3, we consider the simplest cluster approximations with the basic clusters (a), (b) and (c) of Fig. 1 corresponding to the Bragg–Williams [41], Bethe–Peierls [20] and Kramers–Wannier [42] approximations, respectively. The energies $\varepsilon_{\kappa}^{(v)}$ and their multiplicities $\lambda_{\kappa}^{(v)}$ for the topologically inequivalent spin configurations of the isolated clusters are given in Table 1. The consistency relations (2.27) between the distribution numbers $p_{\kappa}^{(v)}$ of the subclusters and the basic clusters $p_{\kappa}^{(w)}$ as well as the dependences of $p_{\kappa}^{(w)}$ on the mutually independent CVM variables x_i for the (w)–clusters are listed in Table 2. Concerning the choice of the variables x_i in proceeding from the (w)–cluster to the ($w+1$)–cluster approximation (e.g. (a) \rightarrow (b)), it is convenient to preserve the definitions of the x_i or, equivalently, the x –dependences of $p_{\kappa}^{(v)}$ with $(v) \subseteq (w)$. Then, only the x –dependences of $p_{\kappa}^{(w+1)}$ have to be determined from the consistency relations. Accordingly, we take the choice $x_1 = p_1^{(a)} - p_2^{(a)}$, $x_2 = p_2^{(b)}$, $x_3 = p_3^{(c)}$, $x_4 = p_4^{(c)}$ and $x_5 = p_2^{(c)} - p_5^{(c)}$.

As can be seen from Table 2, the expectation value $K_{\bar{h}} = \langle s_i \rangle$ is given by $K_{\bar{h}} = x_1$ (being the order parameter in the ferromagnetic Ising model).

The geometrical factors $y_w^{(v)}$ appearing in eq. (2.24) are defined by the set of equations [21]

$$\sum_{v=a}^w \alpha^{(u)(v)} y_w^{(v)} = x^{(u)}; \quad (u) \subseteq (w), \quad (\text{B.1})$$

κ	$(a) = \circ$			$(b) = \circ\text{---}\circ$			$(c) = \begin{array}{c} \circ \\ \text{---} \\ \circ \end{array}$		
		$\lambda_\kappa^{(a)}$	$\varepsilon_\kappa^{(a)}$		$\lambda_\kappa^{(b)}$	$\varepsilon_\kappa^{(b)}$		$\lambda_\kappa^{(c)}$	$\varepsilon_\kappa^{(c)}$
1	\bullet	1	$-\bar{h}$	$\bullet\text{---}\bullet$	1	$-2\bar{h} - \bar{J}_1$	$\begin{array}{c} \bullet \\ \text{---} \\ \bullet \end{array}$	1	$-4\bar{h} - 4\bar{J}_1 - 2\bar{J}_2$
2	\circ	1	\bar{h}	$\bullet\text{---}\circ$	2	\bar{J}_1	$\begin{array}{c} \bullet \\ \text{---} \\ \circ \end{array}$	4	$-2\bar{h}$
3				$\circ\text{---}\circ$	1	$+2\bar{h} - \bar{J}_1$	$\begin{array}{c} \bullet \\ \text{---} \\ \circ \end{array}$	4	$2\bar{J}_2$
4				$\begin{array}{c} \bullet \\ \text{---} \\ \circ \end{array}$	2	$4\bar{J}_1 - 2\bar{J}_2$			
5				$\begin{array}{c} \bullet \\ \text{---} \\ \circ \\ \text{---} \\ \circ \end{array}$	4	$2\bar{h}$			
6				$\begin{array}{c} \circ \\ \text{---} \\ \circ \end{array}$	1	$4\bar{h} - 4\bar{J}_1 - 2\bar{J}_2$			

Tab. 1: The topologically different configurations κ ($\bullet = \uparrow$, $\circ = \downarrow$), multiplicities $\lambda_\kappa^{(v)}$ and configuration energies $\varepsilon_\kappa^{(v)}$ for the clusters (a) , (b) and (c) .

where the matrix element $\alpha^{(u)(v)}$ indicates the number of clusters (u) contained in the cluster (v) and $x^{(u)}$ gives the total number of (u) -clusters in the lattice divided by N .

Let us now exemplify the CVM in the course of successively increasing sizes of the basic cluster (w) .

(i) Bragg–Williams approximation

Taking a single site as basic ‘cluster’, i.e. $(w) = (a)$, from Tables 1 and 2 we obtain the free energy (2.25) as

$$\mathcal{F}^{(a)}(x_1) = -N \left[x_1 \bar{h} - \frac{1}{\beta} \sum_{\kappa=1}^2 p_\kappa^{(a)} \ln p_\kappa^{(a)} \right]. \quad (\text{B.2})$$

Since there are no subclusters and the total number of (a) -clusters in the lattice coincides with N ($x^{(a)} = 1$), from (B.1) we get trivially $y_a^{(a)} = 1$. Thus, the free energy (2.24) in the Bragg–Williams approximation is

$$\mathcal{F}_a(x_1) = \mathcal{F}^{(a)}(x_1). \quad (\text{B.3})$$

The CVM equations (2.28) reduce to the equation $\frac{1}{N} \frac{\partial \mathcal{F}_a}{\partial x_1} = 0$, which, in the paraphase and the $h = 0$ limit, has the solution $x_1 = 0$.

Cluster	consistency relations	CVM variables x_i
(c)	$p_1^{(c)}$	$p_1^{(c)} = \frac{1}{2}(1 + x_1 - 4x_2 + 2x_3 - 2x_5)$
	$p_2^{(c)}$	$p_2^{(c)} = \frac{1}{2}(x_2 - x_3 - x_4 + x_5)$
	$p_3^{(c)}$	$p_3^{(c)} = x_3$
	$p_4^{(c)}$	$p_4^{(c)} = x_4$
	$p_5^{(c)}$	$p_5^{(c)} = \frac{1}{2}(x_2 - x_3 - x_4 - x_5)$
	$p_6^{(c)}$	$p_6^{(c)} = \frac{1}{2}(1 - x_1 - 4x_2 + 2x_3 + 2x_5)$
(b)	$p_1^{(b)} = p_1^{(c)} + 2p_2^{(c)} + p_3^{(c)}$	$p_1^{(b)} = \frac{1}{2}(1 + x_1 - 2x_2)$
	$p_2^{(b)} = p_2^{(c)} + p_3^{(c)} + p_4^{(c)} + p_5^{(c)}$	$p_2^{(b)} = x_2$
	$p_3^{(b)} = p_3^{(c)} + 2p_5^{(c)} + p_6^{(c)}$	$p_3^{(b)} = \frac{1}{2}(1 - x_1 - 2x_2)$
(a)	$p_1^{(a)} = p_1^{(b)} + p_2^{(b)}$	$p_1^{(a)} = \frac{1}{2}(1 + x_1)$
	$p_2^{(a)} = p_2^{(b)} + p_3^{(b)}$	$p_2^{(a)} = \frac{1}{2}(1 - x_1)$

Tab. 2: Distribution numbers $p_\kappa^{(v)}$ of the configurations κ (Table 1) as functions of the distribution numbers of the basic cluster (w) (consistency relations) and as functions of the CVM variables x_i . Note the hierarchy in the choice of x_i (see text).

(ii) Bethe–Peierls approximation

Choosing the cluster (b) as basic cluster (Table 1), the number of relevant spin configurations and CVM variables (Table 2) increases by one. Then, the free energy (2.25) of an assembly of N independent Bethe clusters (b) is obtained as

$$\mathcal{F}^{(b)}(x_1, x_1) = -N \left[2x_1 \bar{h} + (1 - 4x_2) \bar{J}_1 - \frac{1}{\beta} \sum_{\kappa=1}^3 \lambda_\kappa^{(b)} p_\kappa^{(b)} \ln p_\kappa^{(b)} \right]. \quad (\text{B.4})$$

Determining the geometrical factors $y_w^{(v)}$ from (B.1), we note that the cluster (a) is contained twice in (b), and the cluster (b) is contained in the lattice $2N$ times. Accordingly, the equations (B.1) become

$$\begin{pmatrix} 1 & 2 \\ 0 & 1 \end{pmatrix} \begin{pmatrix} y_b^{(a)} \\ y_b^{(b)} \end{pmatrix} = \begin{pmatrix} 1 \\ 2 \end{pmatrix}. \quad (\text{B.5})$$

From the solution of (B.5) and by (2.24) we obtain the free energy in the Bethe–Peierls approximation,

$$\mathcal{F}_b(x_1, x_2) = 2\mathcal{F}^{(b)} - 3\mathcal{F}^{(a)}, \quad (\text{B.6})$$

with $\mathcal{F}^{(b)}$ and $\mathcal{F}^{(a)}$ given by (B.4) and (B.2), respectively.

By (2.31), the nearest–neighbour pair correlation function $K_{\bar{J}_1} = \langle s_i s_j \rangle_1$ is expressed as

$$K_{\bar{J}_1} = 1 - 4x_2. \quad (\text{B.7})$$

Concerning the CVM equations $\frac{1}{N} \frac{\partial \mathcal{F}_b}{\partial x_i} = 0$ ($i = 1, 2$), the equation for x_1 reads

$$-\bar{h} + \frac{1}{\beta} \left[\frac{3}{2} \ln \frac{1-x_1}{1+x_1} + \ln \frac{1+x_1-2x_2}{1-x_1-2x_2} \right] = 0. \quad (\text{B.8})$$

In the paraphase, eq. (B.8) has a non–trivial solution for $h \neq 0$ only and therefore is needed in the calculation of the spin susceptibility (Sec. 4). In the $h = 0$ limit ($x_1 = 0$) there remains the second CVM equation

$$2x_2 I_1^2 = 1 - 2x_2 \quad (\text{B.9})$$

with

$$I_n := \exp \{ \beta \bar{J}_n \}. \quad (\text{B.10})$$

The solution gives

$$x_2 = \frac{1}{4} [1 - \tanh(\beta \bar{J}_1)]. \quad (\text{B.11})$$

Inserting (B.11) into (B.7) one gets the same correlation function $K_{\bar{J}_1}$ as in the original Bethe cluster method (working with an effective Bethe field).

(iii) Kramers–Wannier approximation

Here, the cluster (c) is taken as a basic cluster, and the number of CVM variables is enlarged by three (Tables 1, 2). The free energy (2.25) for (v) = (c) is given by

$$\begin{aligned} \mathcal{F}^{(c)}(x_1, \dots, x_5) = & -N \left\{ 4x_1 \bar{h} + 4(1 - 4x_2) \bar{J}_1 \right. \\ & \left. + 2[1 - 4(x_2 + x_3 - x_4)] \bar{J}_2 - \frac{1}{\beta} \sum_{\kappa=1}^6 \lambda_{\kappa}^{(c)} p_{\kappa}^{(c)} \ln p_{\kappa}^{(c)} \right\}. \quad (\text{B.12}) \end{aligned}$$

From (B.1) we obtain the geometrical factors $y_w^{(v)}$ as solutions of the equations

$$\begin{pmatrix} 1 & 2 & 4 \\ 0 & 1 & 4 \\ 0 & 0 & 1 \end{pmatrix} \begin{pmatrix} y_c^{(a)} \\ y_c^{(b)} \\ y_c^{(c)} \end{pmatrix} = \begin{pmatrix} 1 \\ 2 \\ 1 \end{pmatrix}, \quad (\text{B.13})$$

which yield the free energy in the Kramers–Wannier approximation,

$$\mathcal{F}_c(x_1, \dots, x_5) = \mathcal{F}^{(c)} - 2\mathcal{F}^{(b)} + \mathcal{F}^{(a)}. \quad (\text{B.14})$$

Besides the nearest–neighbour correlation function (B.7), from (2.31), (B.12) and (B.14) the next–nearest–neighbour correlation function

$$K_{\bar{J}_2} = 1 - 4(x_2 + x_3 - x_4) \quad (\text{B.15})$$

can be calculated. In the paraphase and in the $h = 0$ limit, the CVM equations yield $x_1 = x_5 = 0$, and the remaining equations become

$$p_4^{(c)} p_1^{(b)} I_1^2 = p_2^{(c)} p_2^{(b)}, \quad p_3^{(c)} I_2^2 = p_2^{(c)}, \quad p_1^{(c)} p_3^{(c)} p_4^{(c)} = p_2^{(c)2} \quad (\text{B.16})$$

with the distribution numbers taken from Table 2 and the definitions (B.10). Instead of giving the explicit solutions of (B.16), we sketch the resulting zero–temperature behaviour in Fig. 6. There, the degenerate ground–state spin configurations for $h = 0$ are shown in the \bar{J}_1 – \bar{J}_2 plane. For $\bar{J}_2 = 0$, we have antiferromagnetic (π, π) SRO if $\bar{J}_1 < 0$ and ferromagnetic $(0, 0)$ SRO if $\bar{J}_1 > 0$. The inclusion of the next–nearest–neighbour Ising exchange energy \bar{J}_2 gives rise to frustration effects and permits to describe SRO of a stripe structure denoted by $(\pi, 0)$ –SRO.

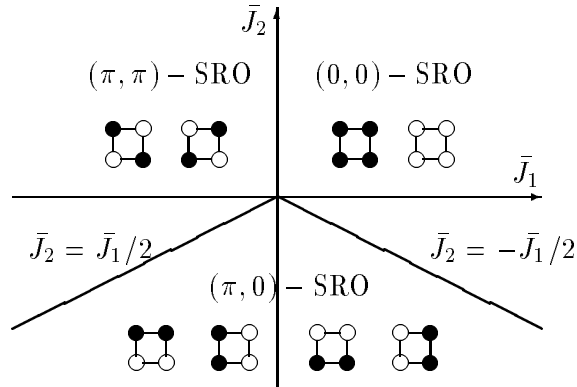


Fig. 6: Paramagnetic solutions of the CVM equations at $T = 0$ within the Kramers–Wannier approximation.

References

- [1] T. Moriya and Y. Takahashi, *J. Phys. Soc. Jpn.* **45**, 397 (1978); T. Moriya and H. Hasegawa, *J. Phys. Soc. Jpn.* **48**, 1490 (1980).
- [2] T. Moriya, p. 2, *Electron Correlation and Magnetism in Narrow-Band Systems*, ed. T. Moriya, volume 29 of *Solid-State Sciences*, Springer-Verlag (Berlin/Heidelberg/New York 1981); T. Moriya, *Spin Fluctuations in Itinerant Electron Magnetism*, volume 56 of *Solid-State Sciences*, Springer-Verlag, (Berlin/Heidelberg/New York 1985).
- [3] V. Korenman, J. L. Murray, and R. E. Prange, *Phys. Rev. B* **16**, 4032, 4048, 4058 (1977).
- [4] R. E. Prange and V. Korenman, *Phys. Rev. B* **19**, 4691, 4698 (1979).
- [5] H. Hasegawa, *Solid State Commun.* **38**, 401 (1981).
- [6] Y. Kakehashi, *J. Phys. Soc. Jpn.* **50**, 1505, 3620 (1981).
- [7] A. P. Kampf, *Physics Reports* **249**, 219 (1994).
- [8] A. P. Kampf, *Phys. Rev. B* **44**, 2637 (1991).
- [9] G. Baumgärtel, J. Schmalian, and K. H. Bennemann, *Europhys. Lett.* **24**, 601 (1993).
- [10] Z. Y. Weng and C. S. Ting, *Phys. Rev. B* **42**, 803 (1990).
- [11] T. Kopp and F. Mila, *Phys. Rev. B* **43**, 12980 (1991); **50**, 13017 (1994).

- [12] U. Trapper, D. Ihle, and H. Fehske, Phys. Rev. B **52**, R 11553 (1995); **54**, 7614 (1996).
- [13] J. Rossat-Mignod et al., Physica B **186–188**, 1 (1993).
- [14] M. Horvatic et al., Physica C **166**, 151 (1990).
- [15] J. B. Torrance et al., Phys. Rev. B **40**, 8872 (1989).
- [16] D. C. Johnston, Phys. Rev. Lett. **62**, 957 (1989).
- [17] M. S. Hybertsen, E. B. Stechel, M. Schlüter, and D. R. Jennison, Phys. Rev. B **41**, 11068 (1990); M. S. Hybertsen, E. B. Stechel, W. M. C. Foulkes, and M. Schlüter, Phys. Rev. B **45**, 10032 (1992).
- [18] E. Sigmund and K. A. Müller, editors, *Phase Separation in Cuprate Superconductors*, Springer-Verlag, (Berlin 1994).
- [19] G. Kotliar and A. E. Ruckenstein, Phys. Rev. Lett. **57**, 1362 (1986).
- [20] H. A. Bethe, Proc. Roy. Soc. London **A150**, 552 (1935); R. Peierls, Proc. Camb. Phil. Soc. **32**, 477 (1936).
- [21] J. Hijmans and J. De Boer, Physica **XXI**, 471, 485, 499 (1955).
- [22] H. Shiba, Prog. Theor. Phys. **46**, 77 (1971).
- [23] H. Hasegawa, J. Phys. Condens. Matter **1**, 9325 (1989).
- [24] H. Fehske, E. Kolley, and W. Kolley, Phys. Status Solidi B **123**, 553 (1984).
- [25] T. Morita, J. Phys. Soc. Jpn. **12**, 753, 1060 (1957).
- [26] M. Deeg, H. Fehske, and H. Büttner, Z. Phys. B **88**, 283 (1992).
- [27] T. Li, P. Wölfle, and P. J. Hirschfeld, Phys. Rev. B **40**, 6817 (1989).
- [28] T. Li, Y. S. Sun, and P. Wölfle, Z. Phys. B **82**, 369 (1991).
- [29] M. Lavagna, Phys. Rev. B **41**, 142 (1990).
- [30] D. M. King et al., Phys. Rev. Lett. **70**, 3159 (1993).
- [31] L. Lilly, A. Muramatsu, and W. Hanke, Phys. Rev. Lett. **65**, 1379 (1990).
- [32] H. Q. Lin and J. E. Hirsch, Phys. Rev. B **35**, 3359 (1987).

- [33] W. Brenig, *J. Low Temp. Phys.* **99**, 319 (1995).
- [34] R. Frésard and P. Wölfle, *Int. J. Mod. Phys. B* **5&6**, 685 (1992).
- [35] D. Duffy and A. Moreo, *cond-mat/9604172* (1996).
- [36] U. Trapper, H. Fehske, and D. Ihle, to be submitted to *Int. Conf. M²S-HTSC-V*, Beijing, China (1997).
- [37] C. Schindelin, U. Trapper, H. Fehske, and H. Büttner, *Czech. J. Physics* **46**, 1881 (1996).
- [38] T. Barnes, *Int. J. Mod. Phys. C* **2**, 659 (1991).
- [39] L. Chen and A.-M. S. Tremblay, *Phys. Rev. B* **49**, 4338 (1994).
- [40] F. Mancini, S. Marra, and H. Matsumoto, *Physica C* **252**, 361 (1995).
- [41] W. L. Bragg and E. J. Williams, *Proc. Roy. Soc. London* **A145**, 699 (1934).
- [42] H. A. Kramers and G. H. Wannier, *Phys. Rev.* **60**, 252, 263 (1941).